CIRA(EXT) 013

October 1996

# Corrections to air kerma rate measurements of $^{137}$Cs environmental sources for free space conditions

D R Shipley
Centre for Ionising Radiation and Acoustics
National Physical Laboratory
Queens Road
Teddington
Middlesex
United Kingdom
TW11 0LW

## ABSTRACT

Air kerma rate measurements between 2 m and 4 m from a set of $^{137}$Cs reference environmental sources (with both stainless steel and brass encapsulation) have been made at NPL using a calibrated Reuter-Stokes high pressure ionisation chamber. Monte Carlo techniques are used to calculate the air kerma rate components over a similar range of distances from these sources. The calculated air kerma values are compared with measurements and the deviation of the data from the inverse square law is investigated. Corrections to the measurement data are then derived to obtain the air kerma rate in free space at 2.5 m from each source.

Simulations of the experimental setup using a collimated $^{137}$Cs environmental source with stainless steel encapsulation reproduce the air kerma rate measurements reasonably well. The calculations indicate that there is a significant contribution to the measured air kerma rate (typically 6%) due to scattered photons and that this contribution does not vary greatly with distance from the source. This scatter contribution is approximately 0.6% greater for sources with brass encapsulation. In both cases, there is approximately a fourfold increase in the scatter component if the beam collimator is removed.

The overall correction (defined as the product of individual corrections for chamber size effect, air attenuation and radiation scatter) to the inverse square law to obtain the air kerma rate in free space at 2.5 m from reference $^{137}$Cs sources with stainless steel and brass encapsulation is 0.961 and 0.955, respectively. The total uncertainty in these corrections is estimated to be 0.27% at the $2\sigma$ level which is much smaller than the estimated random uncertainties in the experimental measurements (which range from 2.6% for the highest activity source to 8.6% for the source with lowest activity).

ISSN 1361-4053

National Physical Laboratory
Teddington, Middlesex, UK, TW11 0LW



Approved on behalf of Managing Director, NPL,
by A J Marks, Director, Centre for Ionising Radiation and Acoustics.

CONTENTS



ILLUSTRATIONS

## TABLES



## APPENDICES

# 1 INTRODUCTION

In the past decade, there has been considerable interest in the monitoring of environmental γ–ray air kerma rates particularly since the incidents at Chernobyl and Three Mile Island. Environmental γ–radiation originates from both natural causes and man-made operations. Natural environmental radiation is predominantly cosmic radiation from outer space and terrestrial radiation from the rocks and soil. It varies (by several orders of magnitude in some cases) with both geographical location and time. The contribution to environmental radiation from man-made operations (such as nuclear power installations) tends to be significantly smaller than from natural radiation and thus can be very difficult to measure. There has therefore been a corresponding growth in interest in the development of specialised monitoring equipment to measure these very small environmental air kerma rates, with traceability to international standards. A EUROMET collaboration has been initiated between the National Physical Laboratory (NPL) and Physikalisch-Technische Bundesanstalt (PTB, Germany) aimed at establishing a UK secondary standard measurement system leading eventually to the launch of a calibration service for environmental dosimetry.

A modular collimated facility has been established at NPL based on low activity $^{137}Cs$ sources. This provides a set of reference dose rates which augment the natural background radiation level in small increments. The output from these sources has been measured using a calibrated high pressure ionisation chamber. Corrections are required to these measurements to characterise the sources in terms of air kerma rate at 2.5 m in free space. The first part of this report describes the air kerma rate measurements that were performed at different distances from the $^{137}Cs$ reference sources. The method used to calculate the air kerma rate components over a similar range of distances from these sources is then discussed. The calculated results are compared with experiment, in the second part of the report, and the deviation of the data from the inverse square law is investigated. Corrections to the measured data are then derived to obtain the air kerma rate in free space at 2.5 m from each of the set of reference sources.

# 2 EXPERIMENTAL MEASUREMENTS

## 2.1 SETUP

The experimental setup for the measurement of air kerma rate under minimal scattering conditions at different distances from reference $^{137}Cs$ environmental sources is shown in Figure 1(a). The sources were mounted on an aluminium source holder which was attached to one end of a standard ISO beam collimator (ISO-4037). The source holder was designed such that the active component of the source capsule lies at the focus of the collimator system. Both source and collimator were then enclosed in lead shielding, as shown, and mounted on a height-adjustable table. A calibrated Reuter-Stokes RSS-112 high pressure ionisation chamber, mounted on a tripod, was positioned at horizontal distances of between 2 m and 4 m from the source. This consists of an 8 litre spherical ionisation chamber with a stainless steel shell (filled with ultra-high purity argon to a pressure of 25 atmospheres) hermetically sealed in a low-humidity box[1]. The chamber had been calibrated in terms of exposure rate over a range of distances between 3 m and 6 m with $^{60}Co$ and $^{226}Ra$ radiation sources traceable to the National Institute of Standards and Technology (NIST). β-rays are not detected by the chamber.

To enable measurements to be performed under conditions of minimal scattering, the apparatus was setup in a large exposure room at the NPL. The exposure room has a floor area of approximately 8 m × 3 m and a height of 3 m. The apparatus was mounted approximately 1 m above the floor of the facility with the source/collimator system at 1 m from an end-wall (see Figure 1(b)).

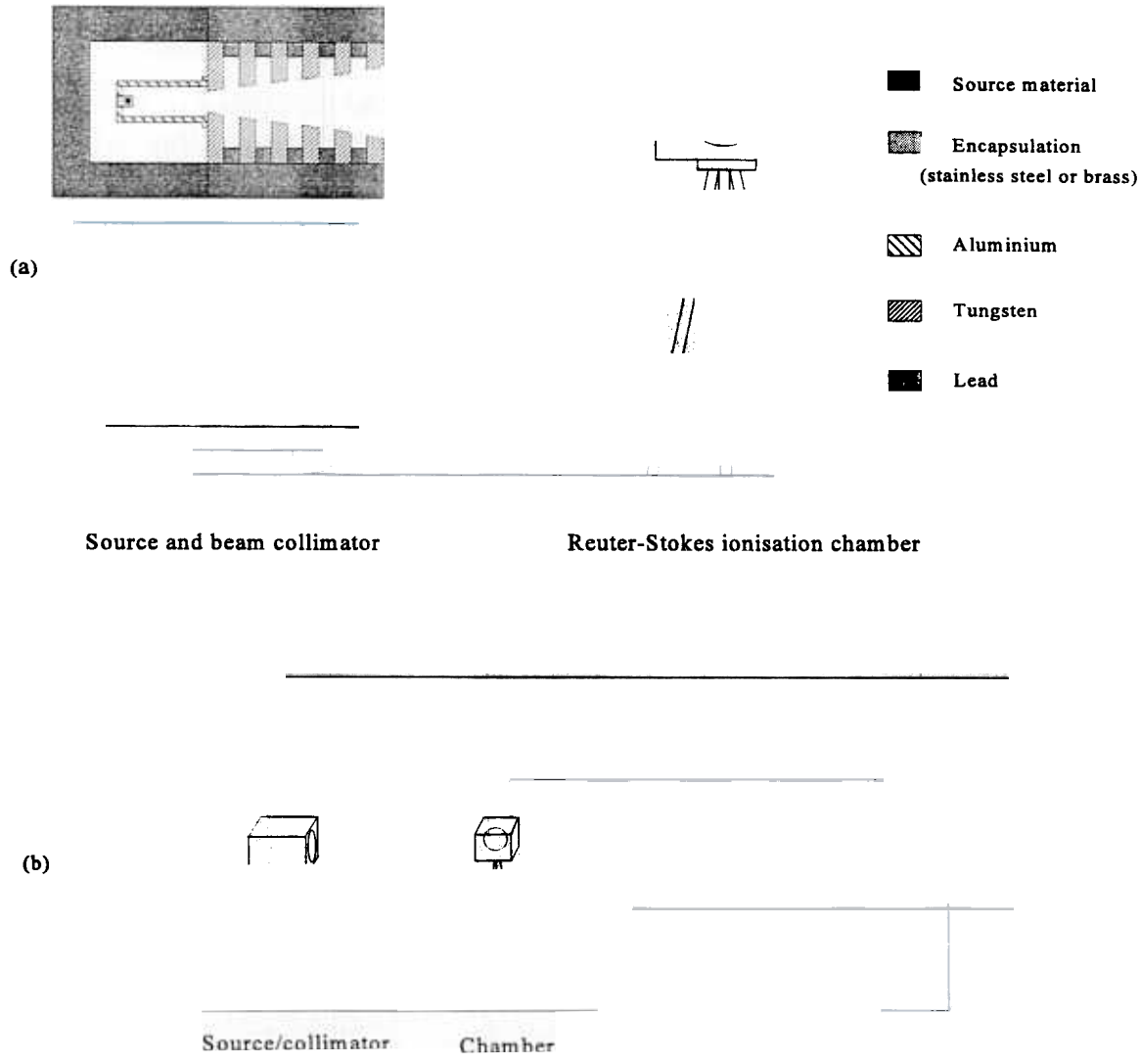


Figure 1 Schematic diagrams showing (a) details of the source setup and the Reuter-Stokes ionisation chamber, and (b) the location of the source assembly and chamber within the experimental facility.

## 2.2 PROCEDURE

A $^{137}Cs$ reference environmental source, supplied by Amersham International plc, with a nominal activity of 9.25 MBq (250 μCi) was used for the bulk of the measurements. The source consists of a small disc (1 mm in thickness and 2.6 mm in diameter) of active caesium metal enclosed in a stainless steel capsule, approximately 18 mm in length and 5 mm in diameter. Exposure rate measurements were made at various distances between 2.0 m and 4.0 m from the source over a period of 5 days[2]. Measurements of background radiation (which form a significant proportion of the measured exposure rate at environmental levels) were also made at regular intervals and their mean subtracted from each source reading. Since the chamber is hermetically sealed from the environment, no correction is required for changes in temperature and atmospheric pressure.

The measurements were then repeated at one distance using the other environmental sources with different nominal activities. These sources are identical in construction to the 9.25 MBq source with the exception that the three lowest activity sources (0.74 MBq, 1.85 MBq and 3.7 MBq) are encapsulated in brass instead of stainless steel.

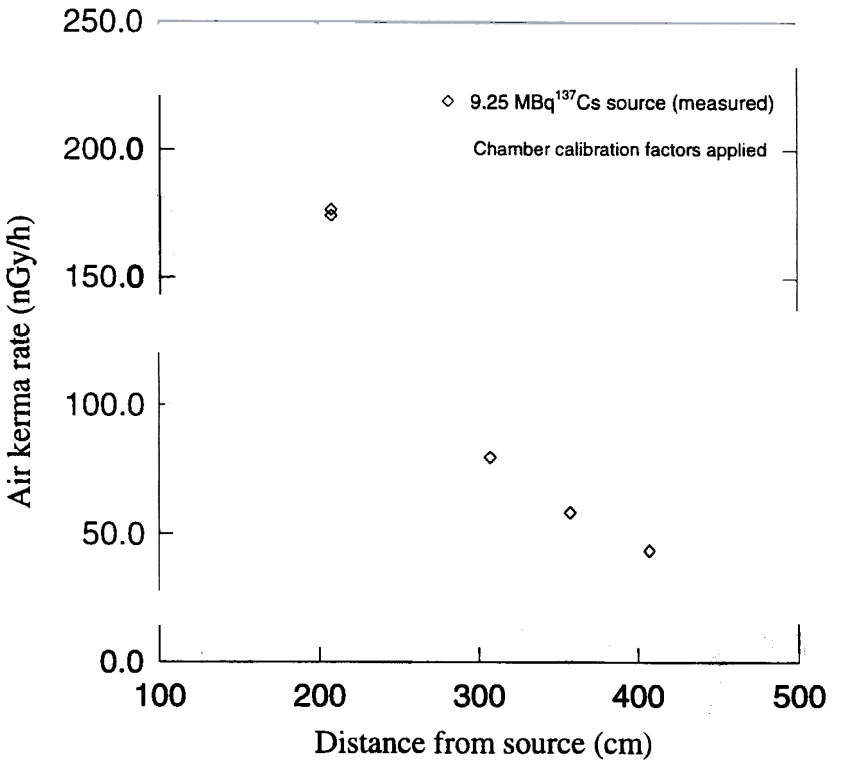


Figure 2 Variation of measured air kerma rate with distance from the 9.25 MBq $^{137}Cs$ environmental source.

## 2.3 RESULTS

The results of the measurements with the 9.25 MBq source are shown in Figure 2, after applying relevant chamber calibration factors and converting the readings from exposure to air kerma. The standard error of the mean for each set of readings was typically better than 0.5% (1σ). The measurements at the minimum and maximum distances from the source were repeated and the observed spread in the mean values was 1.3% and 1.0% respectively. With the lower activity sources, however, spreads of up to 4.3% were obtained in the mean values at a given distance. The significant (and difficult to measure) background component is thought to be likely reason for this large spread in values. For the purpose of this work, the measurement uncertainty was therefore estimated to range from 1.3% (1σ) for the 9.25 MBq source to 4.3% (1σ) for the 0.74 MBq source at all measurement distances. The compliance of the measured data with the inverse-square law will be investigated later in Section 4.

# 3 CALCULATION OF AIR KERMA RATE

## 3.1 THE EGS4 CODE SYSTEM

Most of the calculations described in this report were carried out using the EGS4[1] code system[3]. These codes form a general purpose package for the Monte Carlo simulation of the coupled transport of electrons and photons in an arbitrary geometry for particles with energies ranging from a few keV to several TeV. The package, used in conjunction with a user-written code, calculates the development of an electron-photon cascade from a single incident electron or photon, and transports each particle through the geometry until it reaches a predefined energy cutoff or discard boundary. Electron-photon transport can be simulated in any of 100 elements or mixture of these elements, or any compound. The associated package PEGS4[2], documented

(1) Electron Gamma Shower version 4.

(2) Preprocessor for EGS4.

by Nelson et al.[3], is used to generate datasets of the required materials for subsequent use by EGS4.

## 3.2 METHOD OF CALCULATION

An EGS4 user code XYZCLKER (Version 1.10) was developed to calculate the variation of air kerma rate with distance from a collimated $^{137}$Cs environmental source with both stainless steel and brass encapsulation(3). This code calculates the total air kerma (per initial decay) averaged over 20 cm cubes of air centred at horizontal distances of between 1.0 m and 5.0 m from each source. The kerma due to primary, scattered and Rayleigh scattered photons was also determined in each scoring region (along with their sum as a check on energy conservation). The photon fluence in each scoring region, required in the calculation of air kerma, was determined from the total photon track length divided by the collecting volume. Values for the mass energy absorption coefficient in air, $(\mu_{en}/\rho)_{E,air}$, and fraction of secondary electron energy lost by radiation in air, $g_{air}$, were obtained by log-log interpolation of the tabulated data of Hubbell[4] and Boutillon[5] respectively(4).

The user code models the source and its encapsulation, the source holder and ISO beam collimator very closely with virtually no simplification. The walls, floor and ceiling of the exposure room (which were assumed to be made of concrete) were also included in the simulations since the mean free path of $^{137}$Cs γ-rays in air is significantly greater than the dimensions of the facility. No attempt was made to simulate the effect of the height-adjustable table or other items of equipment present in the room during the measurements.

The coding for the simulation geometry and the material definitions were checked using the program KGCLTEST (Version 1.00) on an Elonex PC-466 personal computer with Lahey F77L-EM/32 Fortran (Version 5.20). This code first places point sources at random in each geometric region and then stores the coordinates of the point of intersection of a randomly-directed 'ray' with the nearest boundary. The outline of each region is then revealed when the points are plotted with an interactive graphics package. The points from regions containing the same material can also be grouped together to enable the distribution of a given material throughout the geometry to be verified.

The datasets required by EGS4 for all the materials in the simulation geometry were generated using PEGS4. In each case, the option to include Rayleigh (coherent) scattering data in the output was also selected to enable the check on energy conservation to be performed (as mentioned earlier).

The EGS4 transport parameters were set to the following values for all regions in the geometry. The minimum (total) electron energy required for explicit δ-ray production, AE, was set to 0.512 MeV, and the minimum (total) energy for electron transport, ECUT, was set to 2.511 MeV. AP and PCUT, the photon equivalents of AE and ECUT, were both set to 0.001 MeV. With these cutoffs, there is no electron transport in the simulations since the electrons are discarded immediately after they are produced. This has no significant effect on the air kerma in each scoring region and greatly reduces the computation time per initial decay.

The photon fluence calculations for sources with stainless steel and brass encapsulation were performed on an HP Apollo 9000/720 workstation using HP FORTRAN/9000 Version 9.0. With the above transport parameters, approximately seven hundred million initial photon decays (at a rate of 11.8 million decays per hour) were required to calculate the total air kerma averaged

---

(3) In all calculations, the γ-ray emissions from each $^{137}$Cs environmental source was assumed to monoenergetic with an energy of 661.660 keV.

(4) The lowest tabulated energy for $g_{air}$ is 0.05 MeV. For photon energies below this energy, $g_{air}$ is assumed be zero.

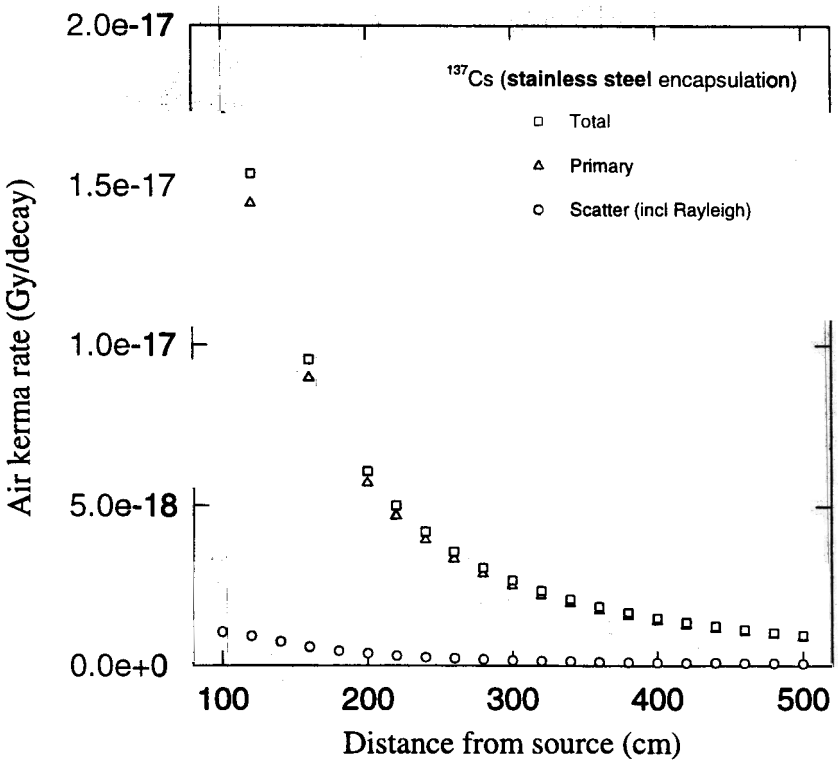


Figure 3 Variation of calculated total, primary and scatter air kerma (per initial decay) with distance from a collimated $^{137}Cs$ environmental source with stainless steel encapsulation.

over a 20 cm cube to a statistical uncertainty at the 1σ level of 0.1% at 1.0 m from the source, and 0.3% at 5.0 m from the source.

### 3.3 RESULTS

The variation of calculated air kerma rate (in Gy per initial decay) with distance for the collimated $^{137}Cs$ environmental source with stainless steel encapsulation is shown in Figure 3. The results are very similar for the collimated source with brass encapsulation (and so have not been shown here). As can be seen, the total and primary air kerma rate decrease with distance in a similar way to the measured air kerma rate (Figure 2). The rate at which these values increase as one approaches the source, however, begins to fall off at distances less than 160 cm. At these distances, the collimated beam does not completely flood the scoring region resulting in a observed reduction in the calculated air kerma rate. The scattered air kerma rate is also significant over this range of distances, forming a slightly greater proportion of the total kerma further from the source. As expected at these energies, less than 1% of the total scatter component is due to Rayleigh-scattered photons. The calculations therefore show that the experimental facility is not quite scatter-free and that corrections may be required to the measured air kerma values to account for this scattered radiation (see Section 4.3).

## 4 DEVIATION FROM THE INVERSE SQUARE LAW

### 4.1 OVERVIEW

The aim of this project was to determine the air kerma rate at 2.5 m from reference $^{137}Cs$ environmental sources under scatter-free conditions. In order to obtain the air kerma rate constant from the measured data, however, a number of corrections are required. A chamber of finite size is used in the experimental measurements, and hence the effective point of measurement is likely to be closer to the source than the geometric centre of the chamber. A correction may therefore be needed to account for this chamber size effect. An air attenuation

correction is also required since the attenuation of the photon fluence between the source and point of measurement is significant at these energies. After allowing for the chamber size effect and air attenuation, the air kerma rate at a given distance from the source should be inversely proportional to the square of the distance from the source, under scatter-free conditions[5]. However, the simulations of the experimental setup have shown that a significant proportion of the measured air kerma rate is due to scattered radiation, and so a further correction to account for this radiation may also needed.

The methods used to determine the corrections for chamber size effect and air attenuation in the experimental measurements are described in Section 4.2. A correction is also required to account for the finite size of the scoring region used in the simulations. This is also discussed in Section 4.2. The correction for radiation scatter is obtained from the simulation results and is discussed in Section 4.3. Although a correction for scatter is required, the correction is small enough that scatter can be neglected in the evaluation of the correction for air attenuation. Likewise, attenuation and scatter are both neglected in the derivation of the chamber size correction. In other words, the combined correction, for attenuation, scatter and chamber size effect are treated independently.

The analysis will concentrate on the measurements carried out with the 9.25 MBq source with stainless steel encapsulation. The same methods will be used to determine the corrections for sources with brass encapsulation with results quoted where necessary. In all cases, the source has been assumed to be point-like. This is a good approximation since the source-chamber distances used in this work are very large compared to the physical size of the source capsule.

## 4.2 CORRECTIONS FOR CHAMBER SIZE AND AIR ATTENUATION

### 4.2.1 Chamber size correction

The Reuter-Stokes RSS-112 ionisation chamber used in the experimental measurements consists of a spherical stainless steel shell (approximately 8 litres in volume) filled with pure argon at a pressure of 25 atmospheres. Based on the known volume of the chamber, the estimated internal diameter of the chamber is therefore 248 mm. Since the diameter of the collecting volume is of the same order of magnitude as the smallest source-chamber distances used in the measurements and the chamber pressure is significantly greater than normal atmospheric pressure, the air kerma rate can vary significantly across the chamber volume due to the diverging photon field. Hence the effective point of measurement and geometric centre of the chamber will not coincide and a correction for chamber size will be required.

For $^{137}$Cs $\gamma$-rays, the CSDA[6] range of secondary electrons in argon at normal atmospheric pressure is approximately 213 cm. If we assume that this range is inversely proportional to the atmospheric pressure then the range in argon at 25 atmospheres is approximately 8.5 cm, which is comparable to the size of the collecting volume of the chamber. The measured ionisation is therefore partly due to electrons generated by photon scattering inside the chamber volume (i.e. the chamber acts like a photon detector) and partly due to electrons originating in the chamber wall (assuming the wall is sufficiently thick for full build-up). An estimate of the chamber size correction for each of these processes will now be derived for the RSS-112 chamber but using air instead of argon in the collecting volume. This change in medium should have no significant effect on the calculated corrections.

For a spherical photon detector of radius $r_s$ centred at a distance $R_0$ from a point source, the air kerma rate $\dot{K}_s$ averaged over the collecting volume, in the absence of attenuation and scatter,

---

(5) This is not the only indication that a correction for radiation scatter is required since the correction itself may be independent of distance from the source.

(6) The range of a particle in the Continuous Slowing Down Approximation.

Table I Estimated chamber size corrections for the Reuter-Stokes RSS-112 ionisation chamber at various source-chamber distances using the photon detector and Kondo and Randolph derivations.

| Source-chamber distance $R_0$ (cm) | $k_{ch}^{PD}$ | $k_{ch}^{KR}$ |
|---|---|---|
| 100 | 0.9969 | 0.9948 |
| 200 | 0.9992 | 0.9987 |
| 250 | 0.9995 | 0.9992 |
| 300 | 0.9997 | 0.9994 |
| 400 | 0.9998 | 0.9997 |
| 500 | 0.9999 | 0.9998 |

may be estimated using the expression (from equation (A9) in Appendix 1):

$$\dot{K}_s \simeq E \frac{\dot{N}(E)}{4\pi\left(R_0^2 - \frac{r_s^2}{5}\right)} \left(\frac{\mu_{en}}{\rho}\right)_{E,air} (1 - g_{air})^{-} \qquad \text{for } r_s < 0.5 R_0 \tag{1}$$

where $\dot{N}(E)$ is the rate at which photons cross a sphere of radius $R_0$ centred at the point source, $(\mu_{en}/\rho)_{E,air}$ is the mass-energy absorption coefficient for air at a photon energy $E$, and $g_{air}$ is the average fraction of secondary electron energy that is lost in radiative interactions along its path in air. The air kerma rate $\dot{K}_0$ at distance $R_0$ from the source is given by (from equation (A6) in Appendix 1):

$$\dot{K}_0 = E \frac{\dot{N}(E)}{4\pi R_0^2} \left(\frac{\mu_{en}}{\rho}\right)_{E,air} (1 - g_{air})^{-1} \tag{2}$$

The chamber size correction, $k_{ch}^{PD}$, required to obtain the actual air kerma rate from the measured air kerma rate at a distance $R_0$ from a point source, using a spherical photon detector of radius $r_s$, is therefore given by the ratio of these expressions:

$$k_{ch}^{PD} \equiv \frac{\dot{K}_0}{\dot{K}_s} = 1 - \frac{r_s^2}{5} \qquad \text{for } r_s < 0.5 R_0 \tag{3}$$

The correction $k_{ch}^{PD}$ is less than unity since the effective point of measurement is closer to the point source than the actual measurement point giving a slightly higher reading for the air kerma rate than required. The estimated chamber size correction, $k_{ch}^{PD}$, for the RSS-112 chamber at different distances from the source is shown in column 2 of Table I.

The effective point of measurement of a spherical chamber in which all the secondary electrons originate from the chamber wall has been considered by Kondo and Randolph[6]. Using their notation, the ratio of air kerma rate measured by the chamber to the air kerma rate at the geometric centre of the chamber, $K$, may be obtained using the expression:

$$K = \frac{1}{2\alpha} \ln\left(\frac{1+\alpha}{1-\alpha}\right) \qquad (>1) \tag{4}$$

where $\alpha$ is the ratio of the internal radius of the chamber to the source-chamber centre distance.

The chamber size correction, $k_{ch}^{KR}$, applicable in this work is therefore obtained from the inverse of $K$, that is:

$$k_{ch}^{KR} = \frac{1}{K} \tag{5}$$

The estimated correction, $k_{ch}^{KR}$, for the RSS-112 chamber at different distances from the source is shown in column 3 of Table I. This method for deriving the chamber size correction was also used by Read et al.[7] for an NPL protection-level secondary standard ionisation chamber in the calibration of $^{60}$Co, $^{226}$Ra and $^{137}$Cs reference sources. Corrections equal to one-half those predicted by Kondo and Randolph were used in that case to produce the best fit to the experimental data, but the full correction was used when the measurements were repeated[8].

The two corrections quoted in Table I at each source-chamber distance represent estimates for the chamber size correction in the extreme cases where the measured ionisation is purely due to electrons generated by photons scattering inside the chamber volume and purely due to electrons originating in the chamber wall. One would therefore expect the required correction, $k_{ch}$, to be close to these values. However, the RSS-112 chamber has been calibrated (in terms of exposure rate) using traceable radiation sources over a range of distances between 3 m and 6 m. The measured calibration factor at these distances (and corresponding factors used at distances closer to source) is therefore likely to include some form of correction for chamber size effect. The actual correction required for the measurements carried out in this work is therefore likely to be smaller than the values quoted in Table I and will mainly account for differences in the correction under measurement and calibration conditions. Under normal circumstances, measurements will only be performed at distances greater than 200 cm from the source to ensure that the collimated beam completely floods the chamber volume. The residual chamber size correction required for measurements at these distances is therefore likely to be much smaller than 0.1% and thus can be ignored. The correction, $k_{ch}$, is therefore taken to be 1.0000 at all measurement distances.

Scoring region size correction

A correction is required to account for the finite size of the cubic scoring regions used in the calculation of air kerma rate. Each scoring region acts like a photon detector and so the correction may be derived using the same method as that used for a spherical photon detector in the previous section. For a cubic photon detector of side $2d$ centred at a distance $R_0$ from a point source, the air kerma rate $\dot{K}_{cube}$ averaged over the volume of the scoring region, in the absence of attenuation and scatter, may be estimated using the expression (from equation (A15) in Appendix 1):

$$\dot{K}_{cube} \approx E \frac{\dot{N}(E)}{4\pi\left(R_0^2 - \frac{d^2}{3}\right)} \left(\frac{\mu_{en}}{\rho}\right)_{E,air} (1 - g_{air}) \qquad \text{for } d < 0.3\,R_0 \tag{6}$$

where $\dot{N}(E)$, $(\mu_{en}/\rho)_{E,air}$ and $g_{air}$ are defined as before. The scoring region size correction, $k_{sr}$, is obtained from the ratio of air kerma rate at distance $R_0$ from the source, $\dot{K}_0$, (equation (A6)) and $\dot{K}_{cube}$, and has the form:

$$k_{sr} \equiv \frac{\dot{K}_0}{\dot{K}_{cube}} = 1 - \frac{d^2}{3R_0^2} \qquad \text{for } d < 0.3\,R_0 \tag{7}$$

The correction $k_{sr}$ ranges from 0.9967 at 100 cm from the source to 0.9999 at 500 cm from the source for the 20 cm cubes used in the simulations.

Air attenuation correction

The air kerma rate $\dot{K}$ due to primary photons at a distance $R_0$ from a point source may be

expressed in the form:

$$\dot{K} = \frac{\dot{K}_0 \exp(-\mu_{air} R_0)}{R_0^2} \quad (8)$$

where $\mu_{air}$ is the narrow-beam attenuation coefficient for air. The air attenuation correction, $k_{att}$ that accounts for the attenuation of the photon beam by the intervening air is therefore:

$$k_{att} = \exp(\mu_{air} R_0) \quad (9)$$

These expressions ignore the buildup factor[9] which takes into account the contribution of scattered photons in $\dot{K}$ (reducing the effective attenuation of the photon beam). This is included in the radiation scatter correction in the present analysis (see Section 4.3). The mass-attenuation coefficients for air, $(\mu/\rho)_{air}$, were obtained using the computer program XCOM[10]. This program generates cross sections and mass attenuation coefficients for any element, compound or mixture at energies between 1 keV and 100 GeV. For $^{137}$Cs γ-rays, $(\mu/\rho)_{air}$ is 0.07718 $cm^2 g^{-1}$ which gives a value for $k_{att}$ of 1.0093 at 100 cm from the source and 1.0476 at 500 cm from the source. The correction is independent of source encapsulation.

### 4.2.4 Comparison of corrected experimental data with calculation

Figure 4 shows the variation of measured air kerma rate normalised to 2.5 m from the collimated $^{137}$Cs source (with stainless steel encapsulation) after correcting for air attenuation ($k_{att}$). The normalisation to 2.5 m is obtained in each case by multiplying the corrected air kerma rate by the square of the ratio of measurement distance to reference distance. As can be seen from the plot, the normalised air kerma rate appears to decrease slightly with distance from the source. However, this may not in fact be the case since the spread in the repeat measurements at each distance is large (ranging from 1–2% with the higher activity sources to 4–5% with the lowest activity source). One would expect the normalised air kerma rate to be independent of distance under scatter-free conditions (or conditions where the radiation scatter component does not vary significantly with distance from the source).

The variation of calculated total and primary air kerma rates, normalised to 2.5 m from the source, is also shown in Figure 4, after correcting for scoring region size ($k_{sr}$) and air attenuation ($k_{att}$). The error bars indicate the statistical uncertainty at the 1σ level. In the figure, the calculated total air kerma values have been matched with the measured data and correspond to a source activity of 8.61 MBq (232.8 μCi). The uncertainty in the source activity at the time of manufacture is the most probable reason why this activity is smaller than the quoted nominal value. From Figure 4, the calculated total air kerma rate (normalised to 2.5 m) appears to be more or less independent of distance from the source (at distances greater than 1.6 m). This is also true for the normalised primary air kerma rate, as one would expect, but at a smaller constant value. These results therefore confirm that the measured data require a correction to account for radiation scatter and also indicate that the correction does not vary greatly over the range of distances considered in this work. The normalised air kerma rates fall rapidly at distances closer than 1.6 m from the source due to the collimated beam not completely flooding the scoring region. The dashed line in the figure indicates the direct value[7] for the air kerma rate at 2.5 m from an isotropic $^{137}$Cs source (in the absence of attenuation and scatter), that is, 115.44 ± 0.58 (1σ) nGy $h^{-1}$. The primary air kerma rate at each distance agrees with this value to within 1-2σ indicating that the calculations of air kerma rate are reliable.

---

[7] The direct calculation of air kerma rate at 2.5 m from the $^{137}$Cs source assumes an activity of 8.61 MBq. Air attenuation and scatter are ignored but attenuation by the source and its encapsulation (0.5 mm caesium metal and 1.0 mm stainless steel) is included. The uncertainty quoted in this value is due to the 0.5% estimated uncertainty in the interpolation of the mass-energy absorption coefficient data, which is indicated in the figure by the two dotted lines on either side of the expected value. The uncertainty in the actual data (~2%) is not included in this value.

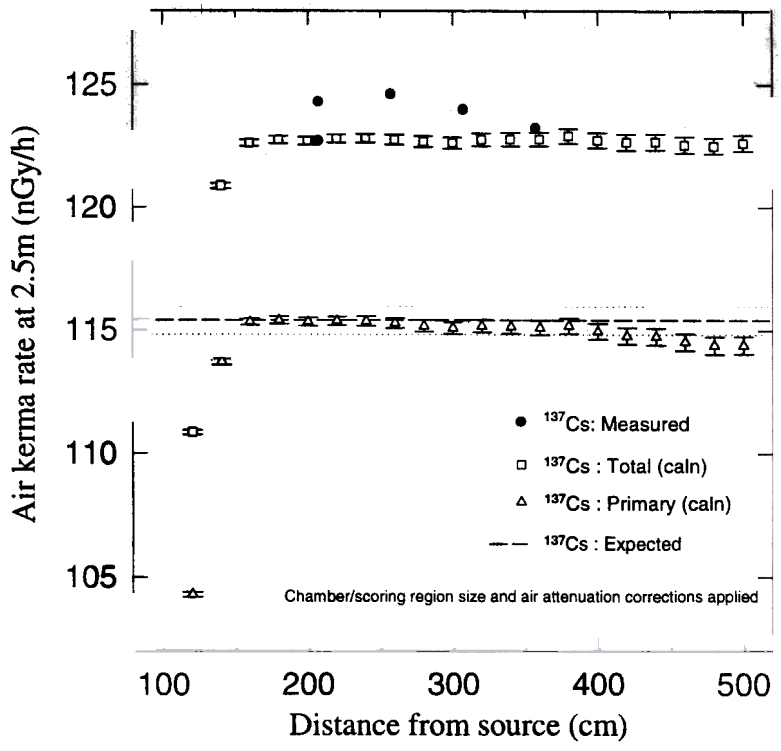


Figure 4 Variation of measured and calculated total and primary air kerma rates, normalised to 2.5 m from the collimated $^{137}Cs$ source with stainless steel encapsulation, after correcting for chamber/scoring region size and air attenuation. The expected value for the air kerma rate at 2.5 m from the $^{137}Cs$ source is also shown with the two lines on either side representing the estimated 1σ uncertainty in this value.

Figure 5 shows the variation of calculated total and primary air kerma rates normalised to 2.5 m from a collimated $^{137}Cs$ source with brass encapsulation, after correcting for scoring region size and air attenuation. These results assume a nominal source activity of 3.70 MBq (100 μCi) and, as can be seen, have very similar features to those shown in Figure 4. Again, the primary air kerma rate agrees with the direct value (49.23 ± 0.25 nGy $h^{-1}$) to within 1–2σ at distances greater than 1.6 m. Measurements over a range of distances using sources with brass encapsulation are not available.

Figure 6 shows the measured and calculated total air kerma rates (normalised to 2.5 m) for the 9.25 MBq source after applying a linear least-squares fit to the data. The gradient and intercept of the fit to the experimental data are (−1.87 ± 0.72) × $10^{-2}$ nGy $h^{-1}$ $cm^{-1}$ and 128.39 ± 2.30 nGy $h^{-1}$ respectively. The gradient and intercept of the fit to the calculated total air kerma rate values (at distances greater than 1.6 m) are (−3.40 ± 2.12) × $10^{-4}$ nGy $h^{-1}$ $cm^{-1}$ and 122.89 ± 0.07 nGy $h^{-1}$ respectively. All uncertainties are quoted at the 1σ level. As expected, the gradient of the experimental data has a large standard error due to the large spread in the measurement values. It differs from the gradient of the calculated data by around 2.5σ. The results of the fit to the calculated data confirm the earlier observation that the normalised total air kerma rate does not vary significantly with distance from the source. The match between the calculated and experimental data is therefore not particularly good (2–3σ) but is sufficient for determining the required radiation scatter corrections for the measured data. For completion, the gradient and intercept of the fit obtained with the brass encapsulated source are (−0.41 ± 1.39) × $10^{-4}$ nGy $h^{-1}$ $cm^{-1}$ and 52.57 ± 0.05 nGy $h^{-1}$ respectively. Again, these results show that the normalised total air kerma rate is virtually independent of distance from the source.

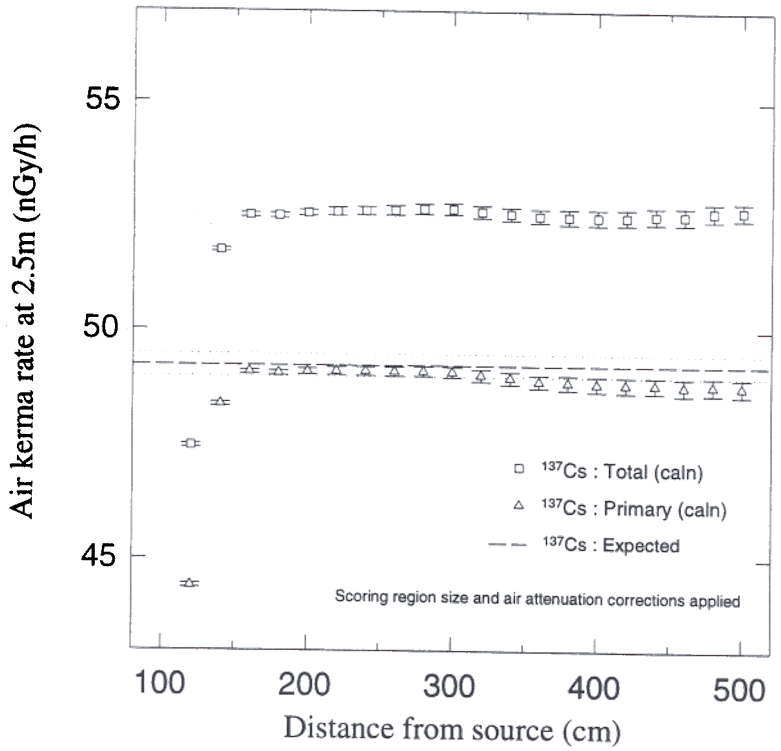


Figure 5 Variation of calculated total and primary air kerma rate, normalised to 2.5 m from the collimated $^{137}Cs$ source with brass encapsulation, after correcting for scoring region size and air attenuation. The expected value for the air kerma rate at 2.5 m from the $^{137}Cs$ source is also shown with the two lines on either side representing the estimated 1σ uncertainty in this value.

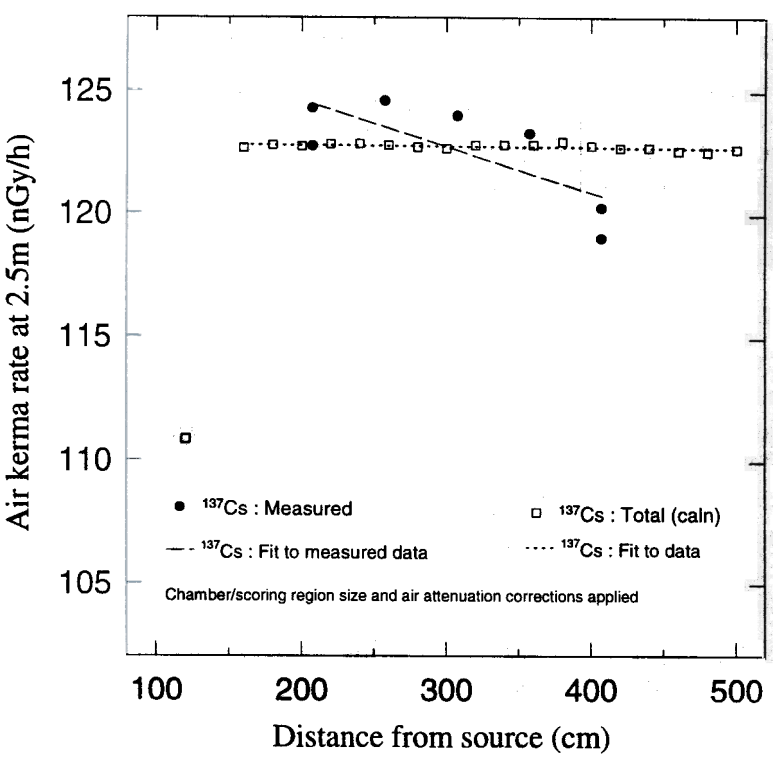


Figure 6 Least-square fits to the measured and calculated total air kerma rates (normalised to 2.5 m from the source).

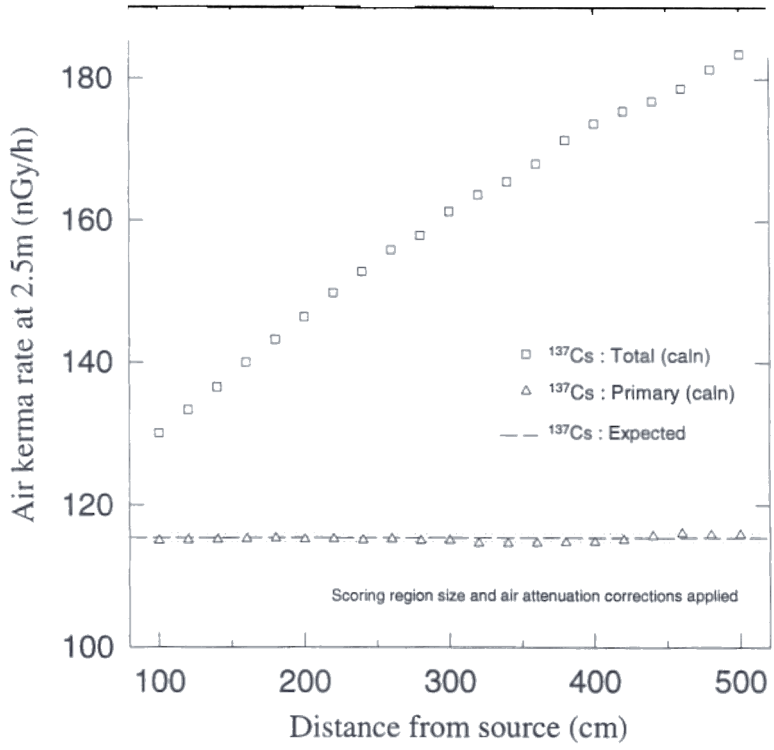


Figure 7 Variation of calculated total and primary air kerma rate, normalised to 2.5 m from the $^{137}$Cs source with stainless steel encapsulation but with no form of collimation, after correcting for scoring region size and air attenuation.

The variation of calculated total and primary air kerma rates (normalised to 2.5 m) from the 9.25 MBq source without any form of collimation is shown in Figure 7, after correcting for scoring region size and air attenuation. With no collimation, the normalised total air kerma rate over this range of distances is generally greater than that obtained with the collimation present (Figure 4), and increases quite rapidly with distance from the source. The normalised primary air kerma rate is more or less independent of distance from the source, as expected, and is in good agreement with the direct value. These results indicate that a larger correction for radiation scatter would be required in this case which increases with distance from the source. The use of a collimator therefore has a dramatic effect on the air kerma rate greatly reducing the scatter component and corresponding radiation scatter correction.

## 4.3 CORRECTION FOR RADIATION SCATTER

The discussion in the previous section has shown that the experimental measurements with collimated $^{137}$Cs environmental sources have been reproduced sufficiently well using Monte Carlo techniques. One can therefore use the simulation results to estimate the correction required to account for radiation scatter in the measurements. If $\dot{K}_{pr}$ is the kerma rate due to primary photons at a point in air at a given distance from the source, and $\dot{K}_{sc}$ is the kerma rate due to scattered photons at that point (whatever their origin), then the total air kerma rate $\dot{K}$ at the point is given by:

$$\dot{K} = \dot{K}_{pr} + \dot{K}_{sc}$$

It then follows that the correction factor $k_{sc}$ required to account for scattered radiation at the point in air has the form:

$$k_{sc} = \frac{\dot{K}_{pr}}{\dot{K}_{pr} + \dot{K}_{sc}} = \frac{\dot{K}_{pr}}{\dot{K}} \qquad (<1)$$

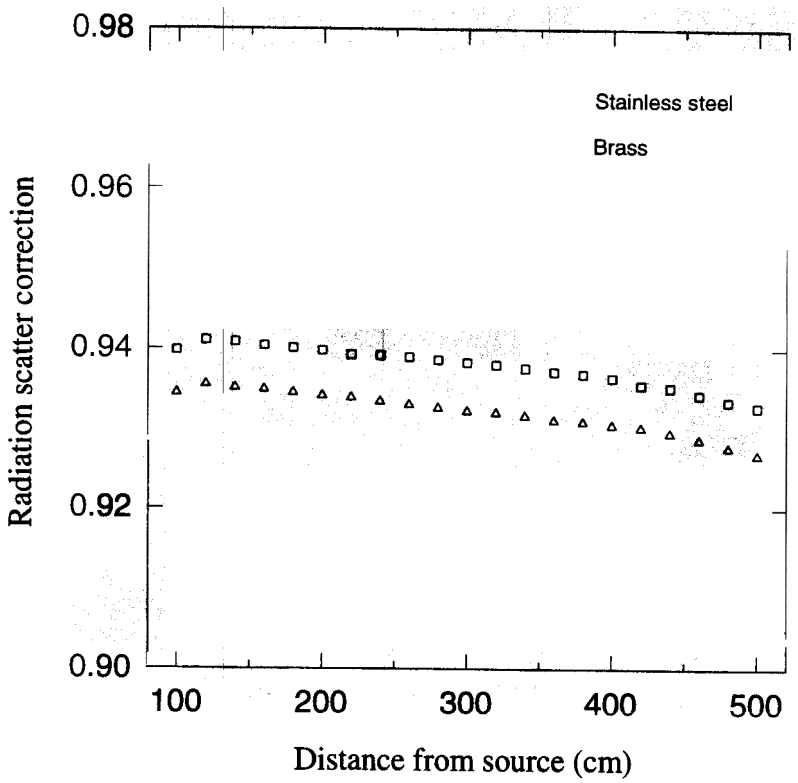


Figure 8 Variation of the radiation scatter correction with distance from the collimated $^{137}Cs$ sources with stainless steel and brass encapsulation.

In this work, the values for $k_{sc}$ required to correct the experimental data were estimated from the ratio of primary and total air kerma rates calculated at different distances from the $^{137}Cs$ sources with stainless steel and brass encapsulation. The variation of $k_{sc}$ with distance from these sources is shown in Figure 8. A least squares fit was applied to each set of points (at distances greater than 1.6 m) to enable $k_{sc}$ to be evaluated at each measurement distance. The gradient and intercept of the fit obtained with the stainless steel encapsulated source are $(-2.110 \pm 0.112) \times 10^{-5}$ cm$^{-1}$ and $0.9442 \pm 0.0004$ respectively. The corresponding gradient and intercept obtained with the brass encapsulated source are $(-2.156 \pm 0.096) \times 10^{-5}$ cm$^{-1}$ and $0.9385 \pm 0.0003$ respectively. The uncertainties in each value are quoted at the 1σ level. These results show that, for both types of source encapsulation, the radiation scatter component decreases only very slightly (~0.8%) over the whole range of distances considered. The correction required for a brass encapsulated source is also approximately 0.6% greater than that required for a stainless steel encapsulated source over these distances. At the reference distance of 2.5 m from the source, $k_{sc}$ has a value of 0.9389 for the stainless steel encapsulated source and 0.9331 for the brass encapsulated source. For comparison, the corresponding correction at this distance for the stainless steel encapsulated source with no collimation is approximately 0.75 (or 25%), confirming that the collimator dramatically reduces radiation scatter.

## 4.4 OVERALL CORRECTION

The overall correction factor $k_{ov}$ at each measurement distance is the product of the corrections for chamber size effect, air attenuation and radiation scatter ($k_{ch} \times k_{att} \times k_{sc}$). The equation of the curve is given by:

$$k_{\cdot} \quad .0 \cdot \exp(\mu_{air} R_0)(a_{sc} + b_{sc} R_0) \tag{12}$$

where $a_{sc}$ and $b_{sc}$ are respectively the intercept and gradient of the least-squares line applied to the data for the radiation scatter correction (see Section 4.3). The chamber size correction, $k_{ch}$,

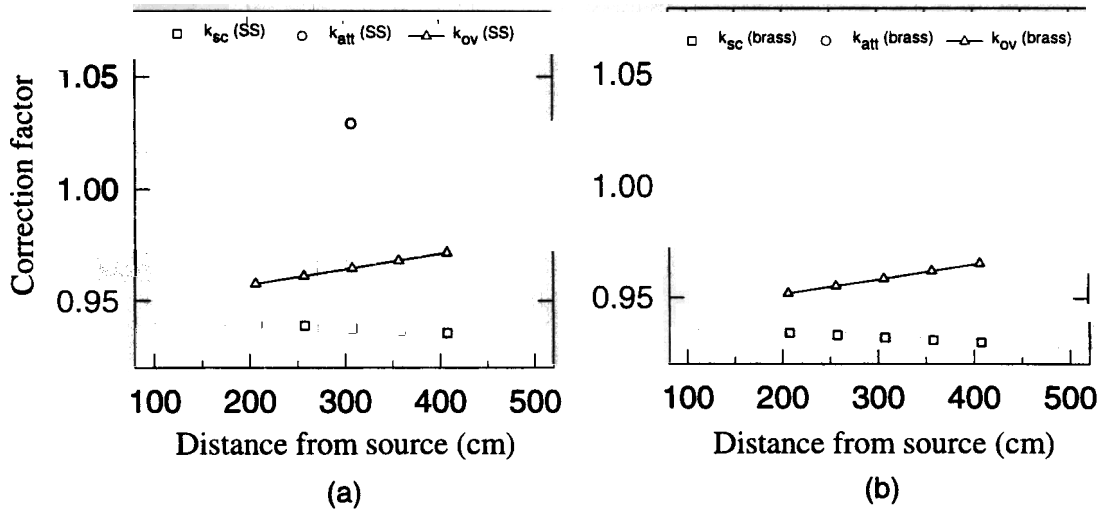


Figure 9 Variation of air attenuation, radiation scatter and overall correction with distance from the collimated $^{137}$Cs source with (a) stainless steel encapsulation, and (b) brass encapsulation.

is taken to be 1.0000 (Section 4.2.1). The variation of $k_{att}$, $k_{sc}$ and $k_{ov}$, for both stainless steel and brass encapsulated sources, over the range of measurement distances considered in this work is shown in Figures 9(a) and 9(b) respectively. In both cases, the radiation scatter correction is larger than the corresponding air attenuation correction (although in the opposite direction) but does not vary as much with distance from the source. The overall correction, $k_{ov}$, is therefore largest at the closest measurement distance but decreases with increasing distance from the source, as shown. The correction required for sources with brass encapsulation is approximately 0.6% greater than that for stainless steel encapsulation over these distances due to the larger scatter component (Section 4.3). Using equation (12), the overall correction at 2.5 m from sources with stainless steel and brass encapsulation is 0.9610 and 0.9551 respectively.

Figure 10 shows the variation with distance of the measured air kerma rate normalised to 2.5 m from the 9.25 MBq source with stainless steel encapsulation, after correcting for chamber size effect, air attenuation and radiation scatter. The expected value for the air kerma rate at 2.5 m from this source (in the absence of attenuation and scatter) is also shown. As can be seen, the corrected air kerma rates are now within 2–3% of the expected value but still do not appear to quite satisfy the inverse-square law. The large spread in the experimental data, due to the difficulty in measuring air kerma rates at environmental levels, is the most probable cause of this slight trend. It is therefore unlikely that any improvement in the agreement between calculation and measurement can be obtained without performing more comprehensive experimental measurements.

## 5 UNCERTAINTIES

The random and systematic uncertainties in the determination of the overall correction factor for measurements with collimated $^{137}$Cs environmental sources will be considered in this section. The quoted uncertainties apply to both stainless steel and brass encapsulated sources. As discussed in Section 2.3, the random uncertainty in the source measurements was estimated from the spread of repeat measurements of air kerma rate at the minimum and maximum distances from the source, that is 2.6% at the 2σ level for the highest activity (9.25 MBq) source. This value seems reasonable since it is roughly equal to the maximum deviation of each measured air kerma rate (after correction) from the expected value, as shown in Figure 10. The random uncertainty in measurements with the lower activity sources are, however, thought to be much greater (up to 8.6% at the 2σ level for the 0.74 MBq source).

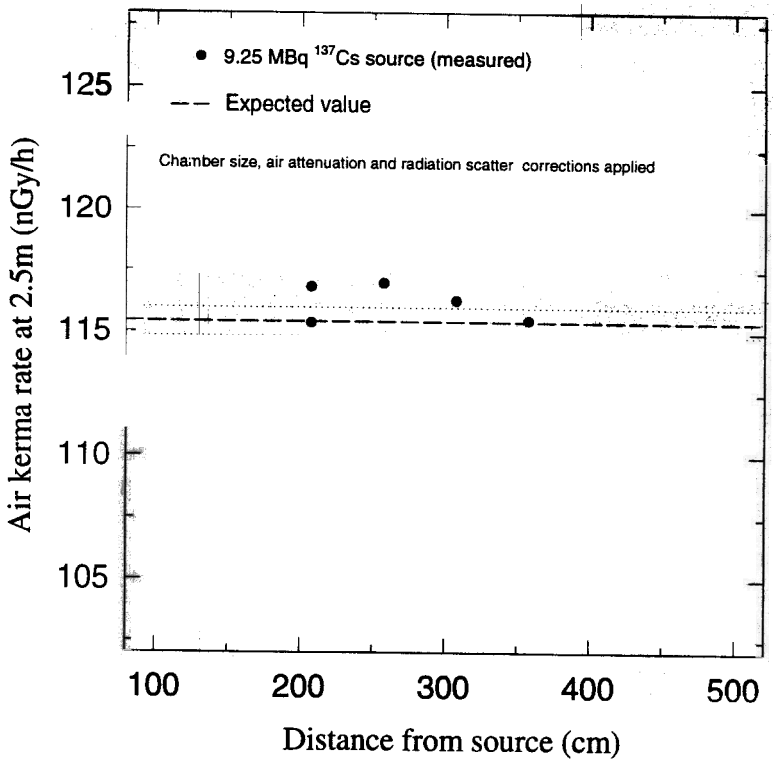


Figure 10 Measured air kerma rate normalised to 2.5 m from the 9.25 MBq source after correcting for chamber size effect, air attenuation and radiation scatter. The expected value for the air kerma rate at 2.5 m from this source is also shown.

There are also a number of systematic uncertainties associated with the individual corrections that make up the overall correction factor. In the determination of the correction for finite chamber size, the analysis has not considered the effect of increased chamber pressure on the value of the correction (apart from the reduced CSDA range of secondary electrons). At a pressure of 25 atmospheres, the attenuation of the photon beam across the chamber diameter increases to around 4% which, using a simple one-dimensional model, corresponds to a displacement of approximately 0.25 cm of the effective centre of the chamber towards the source. However, at this pressure, there is also an increased scatter component within the chamber which partially (but not completely) compensates for this effect. It is therefore difficult to determine the net change in the displacement of the effective centre without performing a more detailed analysis (possibly using Monte Carlo techniques). A value of 0.1% at the $2\sigma$ level is thought to be a reasonable estimate of the systematic uncertainty in this correction (since the correction itself is small ($\lesssim 0.1\%$)).

The major source of uncertainty in the correction for air attenuation is associated with the values used for the mass attenuation coefficient for air. In this work, the computer program XCOM was used to generate the required attenuation coefficients (which, apart from one or two small differences, are virtually identical to those tabulated by Hubbell[4] and Cullen et al.[11]). For $^{137}$Cs $\gamma$-rays in air, more than 99% of photons undergo incoherent (Compton) scattering. The estimated uncertainty in the mass attenuation coefficient data used in this work is therefore approximately equal to the uncertainty in the partial cross section for incoherent scattering at these energies, which is typically 1% or better according to Hubbell. The systematic uncertainty in the air attenuation corrections, which lie in the range 0.9–4.8%, is therefore at most 0.05% at the $2\sigma$ level.

The corrections for radiation scatter were derived from the ratio of primary and total air kerma rates calculated at different distances from each source. There are several factors contributing

to the uncertainty in the calculation of the air kerma rate. There is an estimated 0.5% uncertainty in the interpolation of the mass-energy absorption coefficient data, used to derive the air kerma rate, as well as an estimated 2% uncertainty in the coefficients themselves. Likewise, there is also an estimated 0.5% uncertainty in the interpolation of the $g_{air}$ data as well as a 25% uncertainty in their values. Since the primary and total air kerma rates are correlated in the simulations, these uncertainties mostly cancel out when taking the ratio, leaving an uncertainty of 0.15% (2σ) at worst. The statistical uncertainties in the calculated air kerma rates, however, appear as a systematic uncertainty in the radiation scatter correction. This systematic uncertainty is at most 0.14% at the 2σ level (obtained by taking the largest statistical uncertainties in the scatter and total air kerma rates in quadrature). Finally, there is an estimated systematic uncertainty of 0.1% (2σ) due to the fitting a least squares line to the calculated scatter corrections, and 0.1% (2σ) due to simplifications made in the simulation geometry. The uncertainty in the radiation scatter correction is therefore at most 0.25% at the 2σ level.

The total uncertainty in the overall correction factor is therefore 0.27% at the 2σ level, obtained by taking the random and systematic uncertainties in quadrature, which is much smaller than the estimated random uncertainty in the experimental measurements.

## 6 SUMMARY AND CONCLUSIONS

The measurements of air kerma rate at distances up to 5 m from collimated $^{137}$Cs environmental sources with stainless steel and brass encapsulation can be reproduced sufficiently well using Monte Carlo techniques. These simulations indicate that, after allowing for chamber size effect and air attenuation, there is a significant contribution to the measured air kerma rate by scattered photons, even though the measurements have been performed under minimal scattering conditions. This scatter contribution is approximately 0.6% greater for sources with brass encapsulation than for sources with stainless steel encapsulation over these distances. In all cases, the use of collimation dramatically reduces the radiation scatter component. The primary air kerma rates, also determined in the simulations, obey the inverse square law (after correction) and, when normalised to a distance of 2.5 m from the source, are in close agreement with the expected values at this distance. This indicates that the simulations of the experimental setup using sources with both types of encapsulation are reliable.

Table II summarises the corrections for air attenuation ($k_{att}$) and radiation scatter ($k_{sc}$) required to obtain the air kerma rate at 2.5 m in free space from the measured air kerma rate, for the $^{137}$Cs environmental sources with stainless steel encapsulation considered in this work. Table III gives the corresponding corrections for $^{137}$Cs environmental sources with brass encapsulation. Corrections are applied to the mean air kerma rate measured at each distance and also to the set of readings with the 9.25 MBq source analysed in detail in this report. The chamber size correction ($k_{ch}$) for these measurements is negligible (<0.1%).

The overall correction (which is the product of $k_{ch}$, $k_{att}$ and $k_{sc}$ ) required to the inverse square law at 2.5 m from each source with stainless steel encapsulation is 0.9610, and at 2.5 m from each source with brass encapsulation is 0.9551. The estimated total uncertainty in this correction is 0.27% at the 95% confidence level (taken to be 2σ). This is much smaller than the estimated uncertainties in the experimental measurements which range from 2.6% for the highest activity source to 8.6% for the lowest activity source. The difficulty in measuring air kerma rates at environmental levels (due to the large background component) is the main reason for these large uncertainties and the lack of good agreement between calculation and experiment. Ideally, more comprehensive and detailed experimental measurements should be performed in an attempt to reduce these uncertainties.

Table II Corrections for air attenuation and radiation scatter required to obtain the air kerma rate in free space at 2.5 m for the set of $^{137}Cs$ reference sources with stainless steel encapsulation.

| Nominal activity (MBq) | Distance (cm) | Measured reading (nGy $h^{-1}$) | $k_{att}$ | $k_{sc}$ | Corrected to 2.5 m (nGy $h^{-1}$) |
|---|---|---|---|---|---|
| 5.55 | 257.5 | 67.16 | 1.0242 | 0.9388 | 68.51 |
| 7.40 | 257.5 | 88.49 | 1.0242 | 0.9388 | 90.27 |
| 9.25 | 257.5 | 113.94 | 1.0242 | 0.9388 | 116.23 |
| 9.25 | 207.5 | 174.83 | 1.0195 | 0.9398 | 115.39 |
| | 207.5 | 177.02 | 1.0195 | 0.9398 | 116.84 |
| | 257.5 | 114.69 | 1.0242 | 0.9388 | 116.99 |
| | 307.5 | 79.67 | 1.0290 | 0.9377 | 116.30 |
| | 357.5 | 58.33 | 1.0338 | 0.9366 | 115.51 |
| | 407.5 | 43.15 | 1.0386 | 0.9356 | 111.40 |
| | 407.5 | 43.59 | 1.0386 | 0.9356 | 112.53 |

Table III Corrections for air attenuation and radiation scatter required to obtain the air kerma rate in free space at 2.5 m for the set of $^{137}Cs$ reference sources with brass encapsulation.

| Nominal activity (MBq) | Distance (cm) | Measured reading (nGy $h^{-1}$) | $k_{att}$ | $k_{sc}$ | Corrected to 2.5 m (nGy $h^{-1}$) |
|---|---|---|---|---|---|
| 0.74 | 257.5 | 9.83 | 1.0242 | 0.9330 | 9.97 |
| 1.85 | 257.5 | 25.28 | 1.0242 | 0.9330 | 25.63 |
| 3.70 | 257.5 | 47.40 | 1.0242 | 0.9330 | 48.05 |

## 7 ACKNOWLEDGEMENTS

I would like to thank Simon Duane, Tudor Williams and Graham Bass for their help during the course of this work. I would also like to acknowledge the financial support of the National Measurement System Policy Unit of the UK Department of Trade and Industry.

## 8 REFERENCES


1 REUTER-STOKES INC. RSS-112 PIC environmental radiation monitoring station operational manual. Revision 1.5. March 1991.

2 BASS, G.A. Private communication. 1996.

3 NELSON, W.R., HIRAYAMA, H. and ROGERS, D.W.O. The EGS4 code system. *Report SLAC-265*, Stanford Linear Accelerator Center, Stanford, CA 94305, 1985.

4 HUBBELL, J.H. Photon mass attenuation and energy-absorption coefficients from 1 keV to 20 MeV. *Int. J. Appl. Radiat. Isot.*, 1982, **33**, 1269–1290.

5 BOUTILLON, M. g-values from Berger and Seltzer tables (1982). *Report CCEMRI(I)/85-18*, Comité Consultatif pour les Étalons de Mesure des Rayonnements Ionisants (CCEMRI), Bureau International des Poids et Mesures (BIPM), Sèvres, 1985.

6 KONDO, S. and RANDOLPH, M.L. Effect of finite size of ionisation chambers on measurements of small photon sources. *Radiat. Res.*, 1960, **13**, 37–60.

7 READ, L.R., BURNS, J.E. and LIQUORISH, R.A.C. Exposure-rate calibration of small radioactive sources of $^{60}$Co, $^{226}$Ra and $^{137}$Cs. *Int. J. Appl. Radiat. Isot.*, 1978, **29**, 21–27.

8 ROSSITER, M.J., WILLIAMS, T.T. and BASS, G.A. Air kerma rate calibrations of small sources of $^{60}$Co, $^{137}$Cs, $^{226}$Ra and $^{192}$Ir. *Phys. Med. Biol.*, 1991, **36**, 279–284.

9 BERGER, M.J. *J. Nucl. Med.*, 1968, **9**, Suppl. No. 1.

10 BERGER, M.J. and HUBBELL, J.H. XCOM: Photon cross sections on a personal computer. *Report NBSIR 87-3597*, National Bureau of Standards, Gaithersburg, MD 20899, 1987.

CULLEN, D.E., CHEN, M.H., HUBBELL, J.H., PERKINS, S.T., PLECHATY, E.F., RATHKOPF, J.A. and SCOFIELD, J.H. Tables and graphs of photon-interaction cross sections from 10 eV to 100 GeV derived from the LLNL evaluated photon data library (EPDL). *Report UCRL-50400, Vol. 6, Part A, Rev. 4*, Lawrence Livermore National Laboratory, Livermore, CA 94551, 1989.

**APPENDIX 1** Kerma at a point and averaged over a sphere and over a cube of finite size

An expression for the air kerma from a point source is used in this appendix to derive the response of a spherical and a cubic 'kerma detector'.

## A1.1 KERMA AT A POINT

If $\Psi(E,R)$ is the photon energy fluence at a distance $R$ from an isotropic monoenergetic point source in air, the kerma $K$ is given by:

$$K = \Psi(E,R)\left(\frac{\mu_{tr}}{\rho}\right)_{E,air} \qquad \text{(A1)}$$

where $(\mu_{tr}/\rho)_{E,air}$ is the mass-energy transfer coefficient for air at the photon energy $E$. In terms of the photon fluence $\Phi(E,R)$:

$$K = E\,\Phi(E,R)\left(\frac{\mu_{tr}}{\rho}\right)_{E,air}$$

In the absence of air attenuation and scatter, the photon fluence $\Phi_0(E,R)$ would take the form:

$$\Phi_0(E,R) = \frac{N(E)}{4\pi R^2}$$

where $N(E)$ is the number of photons emitted by the source, and so the kerma $K_0$ in the absence of attenuation and scatter would be:

$$K_0 = E\,\frac{N(E)}{4\pi R^2}\left(\frac{\mu_{tr}}{\rho}\right)_{E,air}$$

The mass-energy transfer coefficient is related to the mass-energy absorption coefficient for air, $(\mu_{en}/\rho)_{E,air}$ by:

$$\left(\frac{\mu_{en}}{\rho}\right)_{E,air} = (1-g_{air})\left(\frac{\mu_{tr}}{\rho}\right)_{E,air}$$

where $g_{air}$ represents the average fraction of secondary electron energy that is lost in radiative interactions along its path in air.The kerma $K_0$ then becomes:

$$K_0 = E\,\frac{N(E)}{4\pi R^2}\left(\frac{\mu_{en}}{\rho}\right)_{E,air}(1-g_{air})^{-1}$$

Naturally, the kerma in free space decreases with the square of the distance from the source (the inverse-square law).

## A1.2 KERMA IN A SPHERE OF FINITE SIZE

Consider a spherical kerma detector, of radius $r_S$, centred at point $P_0$ at a distance $R_0$ from the source (Figure A1). When $r_S$ has the same order of magnitude as $R_0$, the kerma at different points within the spherical volume will vary significantly due to the diverging photon fluence. In particular, the region closer to the point source will contribute more to the average kerma than the region further away from the source. As a result, the effective centre of the sphere and the geometric centre will not coincide. The average kerma $K_{sph}$ in the sphere can be written as an integral over the volume of the sphere:

$$K_{sph} = \frac{3}{4\pi r_S^3}\int_{sphere} E\,\frac{N(E)}{4\pi R^2}\left(\frac{\mu_{en}}{\rho}\right)_{E,air}(1-g_{air})^{-1}\,d^3R$$

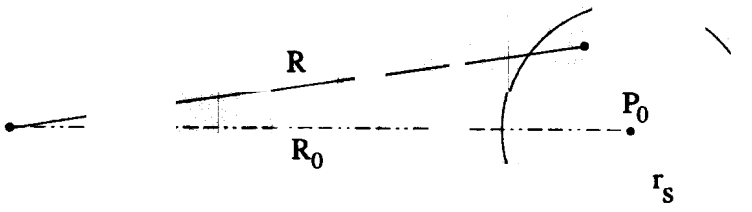


Figure A1 Spherical kerma detector.

Evaluating this integral[8] leads to the expression:

$$K_{sph} = E\frac{N(E)}{4\pi}\left(\frac{\mu_{en}}{\rho}\right)_{E,air}(1-g_{air})^{-1}\frac{1}{R_0^2}\left(1+\frac{1}{5R_0^2}r_S^2+\frac{3}{35R_0^4}r_S^4+O(r_S^6)\right)$$

If $r_S < 0.5R_0$, the second order is sufficient for most kerma calculations (the fourth order term providing a correction smaller than 1%), in which case:

$$\simeq E\frac{N(E)}{4\pi\left(R_0^2-\frac{r_S^2}{5}\right)}\left(\frac{\mu_{en}}{\rho}\right)_{E,air}(1-g_{air})^{-1} \qquad \text{(A9)}$$

So a spherical kerma detector of finite size has an effective centre displaced somewhat towards the source compared to the geometric centre. The displacement Δ varies with distance $R_0$ such that:

$$(R_0-\Delta)^2 \simeq R_0^2-\frac{r_S^2}{5} \qquad \text{(A10)}$$

Solving for Δ gives:

$$\Delta = R_0-\sqrt{R_0^2-\frac{r_S^2}{5}} \qquad \text{(A11)}$$

which can be simplified using a series expansion to:

$$\Delta \simeq \frac{r_S^2}{10R_0} \qquad \text{(A12)}$$

As one would expect, there is no displacement when $r_S = 0$.

## A1.3 KERMA IN A CUBE OF FINITE SIZE

The response of a cubic kerma detector is determined in a same way as for a spherical detector (Section A1.2). For a cube of side $2d$ centered at point $P_0$ in homogeneous air at a distance $R_0$ from the point source (Figure A2), the kerma $K_{cube}$ averaged over the volume of the cube is:

[8] One of the three integrals can be done analytically, the other two require series expansions.

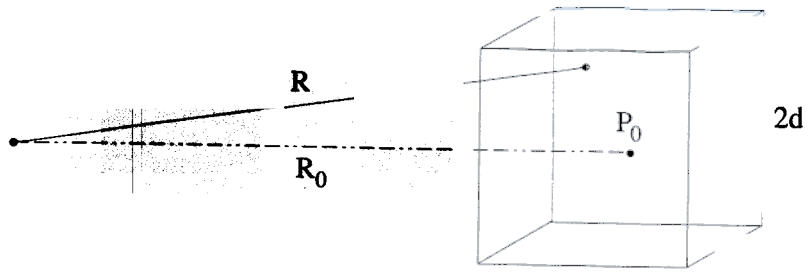


Figure A2 Cubic kerma detector.

$$K_{\text{cube}} = \frac{1}{8d^3} \int_{\text{cube}} E \frac{N(E)}{4\pi R^2} \left( \frac{\mu_{\text{en}}}{\rho} \right)_{\text{E,air}} (1 - g_{\text{air}})^{-1} \, \mathrm{d}^3 R$$

Evaluating $K_{\text{cube}}$ using series expansions gives:

$$K_{\text{cube}} = E \frac{N(E)}{4\pi} \left( \frac{\mu_{\text{en}}}{\rho} \right)_{\text{E,air}} (1 - g_{\text{air}})^{-1} \frac{1}{R_0^2} \left( 1 + \frac{1}{3R_0^2} d^2 - \frac{3}{5R_0^4} d^4 + O(d^6) \right)$$

and, in the case when $d < 3R_0$, this can be re-expressed in the form:

$$K_{\text{cube}} \simeq E \frac{N(E)}{4\pi \left( R^2 - \frac{d^2}{3} \right)} \left( \frac{\mu_{\text{en}}}{\rho} \right)_{\text{E,air}} (1 - g_{\text{air}})^{-1} \qquad \text{for } d < 0.3R_0 \qquad \text{(A15)}$$

This expression is only slightly different to the kerma averaged over a sphere (equation (A9)), and matches the kerma at a point (equation (A6)) when $d$ is set to zero. The displacement $\Delta$ of the effective centre of the cubic detector from its geometric centre is:

$$\Delta \simeq \frac{d^2}{6R_0} \qquad \text{(A16)}$$

which is obtained in the same way as before.